pISSN 1229-3008 eISSN 2287-6251
Progress in Superconductivity and Cryogenics
Vol.20, No.3, (2018), pp.21~27 https://doi.org/10.9714/psac.2018.19.3.021

Numerical and experimental studies of cryogenic reciprocating expander without inner piston

Sehyeon Park[*,a], Junhyuk Bae[a], Kyoungjoong Kim[a], and Sangkwon Jeong[a]

[a] *Korea Advanced Institute of Science and Technology (KAIST), Daejeon, Korea*

(Received 13 February 2018; revised or reviewed 5 September 2018; accepted 6 September 2018)

Abstract

It is difficult to fabricate and maintain moving parts of expander at cryogenic temperature. This paper describes numerical analysis and experimental investigation on a cryogenic reciprocating expander without moving piston. An intake valve which takes high-pressure gas, and an exhaust valve which discharges low-pressure gas, are connected to a tube. The inside pressure of the tube is pulsated for work production. This geometric configuration is similar to that of pulse tube refrigerator but without regenerator. An orifice valve and a reservoir are installed to control the phase of the mass flow and the pressure. At the warm end, a heat exchanger rejects the heat which is converted from the produced work of the expanded gas. For the numerical analysis, mass conservation, energy conservation, and local mass function for valves are used as the governing equations. Before performing cryogenic experiments, we carried out the expander test at room temperature and compared the performance results with the numerical results. For cryogenic experiments, the gas is pre-cooled by liquid nitrogen, and then it enters the pulse tube expander. The experiments are controlled by the opening of the orifice valve. Numerical analysis also found the expander conditions that optimize the expander performance by changing the intake pressure and valve timing as well as the opening of the orifice valve. This paper discusses the experimental data and the numerical analysis results to understand the fundamental behavior of such a newly developed non-mechanical expander and elucidate its potential feature for cryogenic application.

Keywords: pulse tube expander, phase controller, numerical model, warm end heat exchanger, cryogenic

1. INTRODUCTION

In a typical reciprocating expander, there is a piston and a mechanical connection inside the cylinder. The motion of the piston is elaborately controlled by the mechanical connection to produce work effectively. As a result, the piston reciprocates in the cylinder while expanding the internal gas and extracting work. This has the advantage that it is easy to predict the performance by its simple operation. It contains, however, many mechanical moving parts inside the cylinder that cause irreversible loss due to friction and low reliability. This kind of reciprocating expander has a disadvantage in that it is difficult to manufacture and also maintain [1]. In order to overcome such disadvantages, a free-piston reciprocating expander in which a mechanical connection is removed has been developed. In a free-piston reciprocating expander, the movement of the piston is controlled by the pressure difference on both sides of the piston, unlike a typical reciprocating expander in which the mechanical connection controls the movement of the piston.

In 2004, MIT & AMTI developed a free-piston reciprocating expander for a small-scale Collins type 10 K cryocooler for space applications, one of the representative studies on free-piston reciprocating expander. The schematic of the expander is shown in Fig 1. (a). The four solenoid valves are operated at regular time intervals to generate mass flow at each valve, then, the pressure difference on both sides of piston is adjusted [2]. J. Cha developed a free-piston reciprocating expander, replacing four reservoirs and solenoid valves with a reservoir and a single orifice valve that can adjust the opening, in 2016. The schematic of the expander is shown in Fig 1. (b). Similarly, a mass flow is generated through the orifice valve, then, the pressure difference on both sides of the piston is controlled [3].

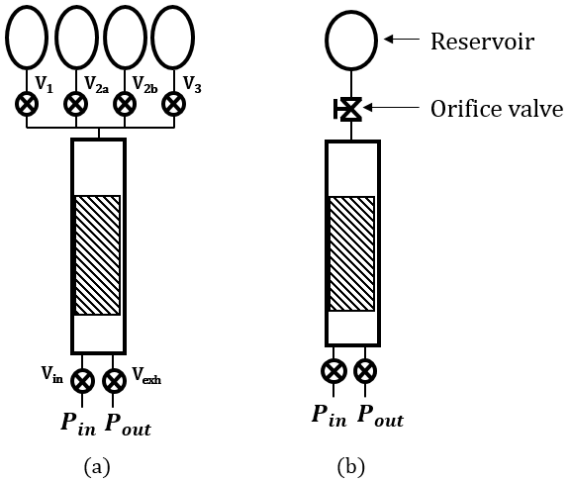

Fig. 1. Schematic diagram of (a) floating piston expander and (b) phase controller expander [3].

* Corresponding author: tpgus9404@kaist.ac.kr

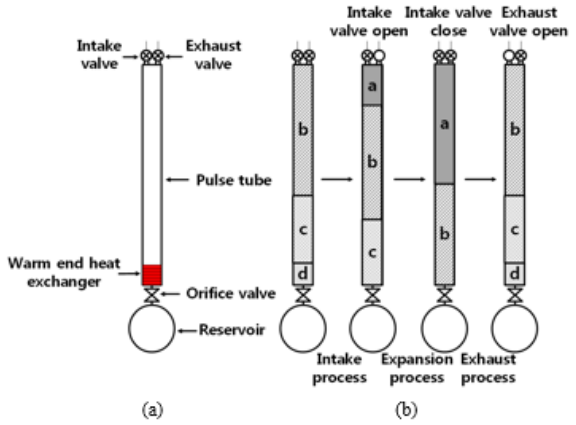

Fig. 2. (a) The schematic of the reciprocating expander without inner piston and (b) operating process.

The combination of such an orifice valve and reservoir is called a phase controller. The free-piston reciprocating expander reduces the friction loss by eliminating the mechanical connection with the piston. However, since the piston, which is a mechanical moving part, still exists inside the cylinder, friction loss and the manufacturing difficulty remains. Therefore, we develop a reciprocating expander in which the piston is completely removed. The role of a piston in a typical expander is replaced by a compressible gas column [4, 5].

The schematic diagram of the expander proposed in this study is shown in Fig 2. (a). An intake valve which takes high-pressure gas, and an exhaust valve which discharges low-pressure gas, are installed at one side. The cylinder in typical expander is replaced by pulse tube, which has relatively small diameter and long length; 50 mm in length and 12.1 mm in inner-diameter. Repeating the operation process, the temperature of the end of the pulse tube nearby the valves decreases and the temperature at the opposite end increases. Therefore, they are respectively called 'cold end' and 'warm end'. The phase controller consisting of an orifice valve with maximum diameter of 3 mm and reservoir with volume of 500 cm^3 are also installed at the pulse tube, and the warm end heat exchanger is installed at the warm end to reject the heat which is converted from the produced work of the expanded gas. The warm end heat exchanger is cooled by cooling water [6, 7].

The schematic of the operating process is shown in Fig 2. (b). The operation principle of the expander is composed of three processes. First, the intake valve is opened. High-pressure gas enters through the intake valve (a). Then, the incoming gas (a) pushes the gas remaining in the pulse tube (b, c, d). A small amount of gas (d) moves to the phase controller. This process is called the intake process. Next, the intake valve is closed. There is no incoming gas anymore. The gas packets in the pulse tube (a, b c) move toward the warm end due to the pressure difference between the pulse tube and the reservoir. And, some gas (c) also moves to the phase controller. This second process is called the expansion process because the entered gas expands as the pressure decreases. Finally, the exhaust valve is opened. The high-pressure gas in the pulse tube (a) exhausts to the low-pressure exit through the exhaust valve. Some of the gas packets (c, d) move from the reservoir to the pulse tube. This final process is called the exhaust process.

2. NUMERICAL ANALYSIS

To analyze the performance characteristic of the expander, the numerical model is set up. There are several assumptions in the modeling. First, the working fluid behaves as an ideal gas. Second, the working fluid moves one-dimensionally only. Third, the pressure gradient in the pulse tube is neglected. Finally, the temperature of the warm end heat exchanger and the reservoir is almost constant at ambient temperature [8]. For the numerical model, the following equations are used. Equation (1) is the mass conservation, equation (2) is the energy conservation and equation (3) is the local mass function for valves [9, 10].

$$\frac{\partial \rho}{\partial t} + \frac{\partial}{\partial x}\left(\frac{\dot{m}}{A_g}\right) = 0 \tag{1}$$

$$\frac{\partial}{\partial t}\left(\rho C_v T_g\right) + \frac{\partial}{\partial x}\left(\frac{\dot{m} C_p T_g}{A_g}\right) + \frac{hA_s}{V}\left(T_g - T_w\right) = 0 \tag{2}$$

Due to the ideal gas assumption, equation (2) can be transformed as follows.

$$\frac{C_v}{R}\cdot\frac{\partial P}{\partial t} + \frac{\partial}{\partial x}\left(\frac{\dot{m} C_p T_g}{A_g}\right) + \frac{hA_s}{V}\left(T_g - T_w\right) = 0 \tag{2-1}$$

$$\dot{m} = f_c \cdot P_{in} \cdot \left(\frac{2k}{k-1}\left(\frac{P}{P_{in}}\right)^{2/k}\left(1 - \left(\frac{P}{P_{in}}\right)^{(k-1)/k}\right)\right)^{1/2} \tag{3}$$

The third term in equation (2-1) indicates the heat transfer to the wall surface. In this case, to obtain the value of f heat transfer coefficient h, Nusselt number (Nu) is calculated according to Reynolds number (Re) as following equation (4) and equation (5). The term f_c in equation (3) means the correction factor and this is determined by comparing experimental and numerical values using trial and error method.

(i) For laminar flow

$$Nu_D = 3.66 + \frac{0.0668 Gz_D}{1 + 0.04 Gz_D^{2/3}} \left(\mathrm{Re}_D < 2300\right) \tag{4}$$

(ii) For turbulent flow

$$Nu_D = \frac{(\frac{f}{8})(\mathrm{Re}_D - 1000)\,\mathrm{Pr}}{1 + 12.7(\frac{f}{8})^{1/2}(\mathrm{Pr}^{2/3} - 1)} \left(\mathrm{Re}_D > 2300\right) \tag{5}$$

$$f = \left(0.079 \ln(\mathrm{Re}_D) - 1.64\right)^{-2} \tag{6}$$

In order to calculate the temperature of the wall surface, the energy conservation equation of the wall surface is used as following equation (7)

$$hA_s\left(T_g - T_w\right) + k_w A_w \frac{\partial T_w}{\partial x} = M_w C_w \frac{\partial T_w}{\partial t} \tag{7}$$

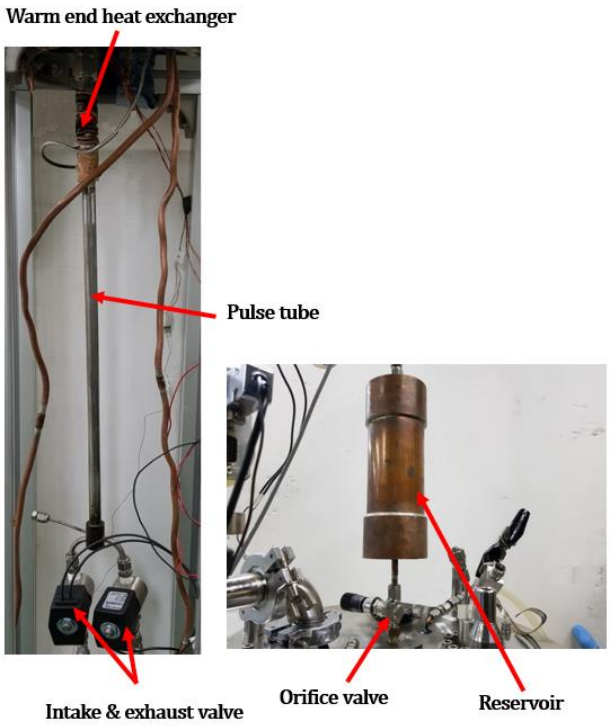

Fig. 3. Experimental apparatus (a) below top flange & (b) above top flange.

3. EXPERIMENTAL APPARATUS

The experimental apparatus is shown in Fig. 3. The experimental apparatus is divided into the lower part (Fig. 3. (a)) and the upper part (Fig. 3. (b)) with reference to the top-flange. The lower part consists of a pulse tube, an intake and exhaust valve, and the warm end heat exchanger with a cooling water line. The pulse tube is made of stainless steel to minimize heat conduction losses. The outer diameter is 12.7 mm, the inner diameter is 12.1 mm. The intake and exhaust valves are solenoid valves (STH12C301T2S, Syntec Korea). Opening and closing each solenoid valve are controlled by transmitting a square wave with constant period through the LabVIEW and DAQ. The warm end heat exchanger is made of a brass rod having a diameter of 15 mm and a length of 70 mm. A brass rod with a hole, having a diameter of 12.7 mm and a depth of 10 mm, is soldered with pulse tube. A hole with a diameter of 12.1 mm and a depth of 50 mm is drilled in the middle part of the brass rod and copper wire meshes having a diameter of 12 mm are soldered at this part. In addition, the cooling water line for the warm end heat exchanger is made of a copper tube having an outer diameter of 3.18 mm and joins to the side of the warm end heat exchanger by soldering. Two temperature sensors (DT-670 SD Type, Lakeshore) are installed before the intake valve and after the exhaust valve to measure the temperature of the intake and exhaust gas. Above the top-flange, a reservoir with a volume of 500 cm^3 and orifice valve (SS-4L-MH, Swagelok) are connected. Pressure sensors (FPA, SENSOTEC) are installed at the pulse tube and the reservoir, and the pressure of each part is measured.

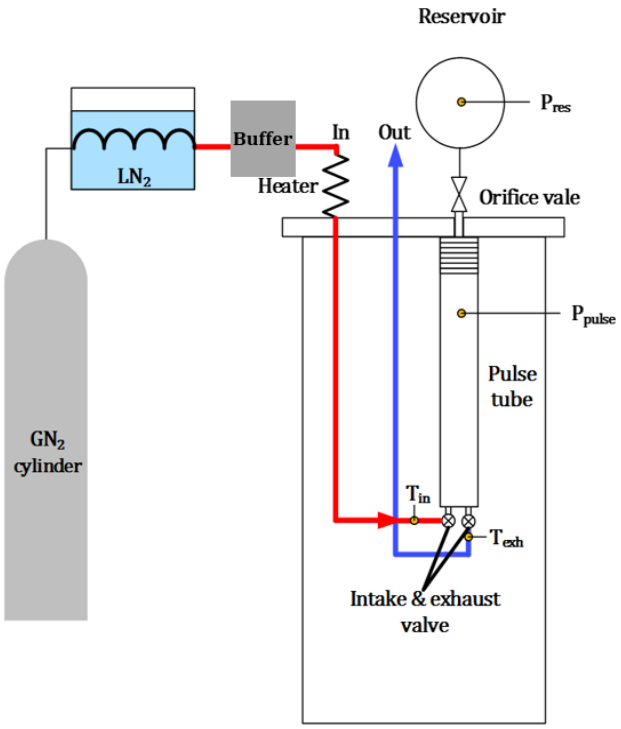

Fig. 4. Schematic of experimental apparatus.

The experiment is conducted with an open cycle. In a nitrogen gas bombe, a high pressure gas is supplied and the pressure of the gas is regulated by a regulator. After passing through the regulator, a buffer, made of stainless steel, having a volume of 500 cm^3 is installed to supply a gas at a constant pressure. At the low temperature experiment, the coil type copper heat exchanger is installed after passing the buffer. In order to supply the low temperature gas to the intake valve, it partially submerges in the liquid nitrogen. Also, for supplying the constant temperature gas, a Nichrome wire is wound around the intake line. During the experiment, the inside of the cryostat is kept in a vacuum state by using a vacuum pump. Experiments are performed until a cyclic steady state is reached, and pressure and temperature data are recorded at a rate of 100 per second by a DAQ (NI USB-6216, National Instruments). The entire experimental apparatus is depicted in Fig. 4.

4. COMPARISON OF EXPERIMENTAL RESULTS AND NUMERICAL ANALYSIS

4.1. Experiment and numerical analysis at ambient temperature

The room temperature experiment conditions are shown in TABLE 1. For the case where the opening degree of the orifice valve is 50 %, the pressure variation during one cycle in cyclic steady state is shown in Fig 5. The average exhaust temperature according to the opening degree of the orifice valve is measured and compared with calculation results as shown in Fig . 6. From the experimental results, it is confirmed that the numerical analysis reasonably predicts the exhaust temperature according to the opening degree of the orifice valve in cyclic steady state.

TABLE 1
NUMERICAL AND EXPERIMENTAL CONDITIONS AT AMBIENT TEMPERATURE.

Variable		Value
pulse tube	inner diameter	12.1 mm
	length	500 mm
	thickness	0.3 mm
	material	stainless steel
reservoir volume		500 cm³
diameter of intake valve		3 mm
diameter of exhaust valve		3 mm
initial temperature and pressure in reservoir & pulse tube		1 Bar/ 300 K
intake/ expansion/ exhaust time		0.06/ 0.12/ 0.18 s
high pressure/ low pressure		900 kPa/ 100 kPa
intake temperature		292 K
working fluid		gas nitrogen
diameter and opening degree of the orifice valve		1.42 mm 0, 20, 50, 80, 100 %

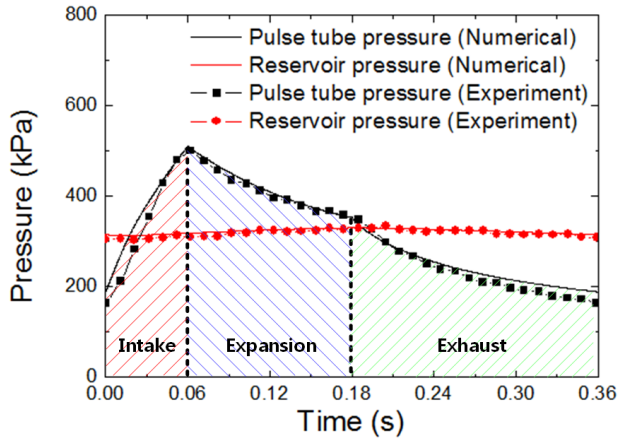

Fig. 5. Pressure during one cycle in cyclic steady state. (opening degree of orifice valve, 50 %)

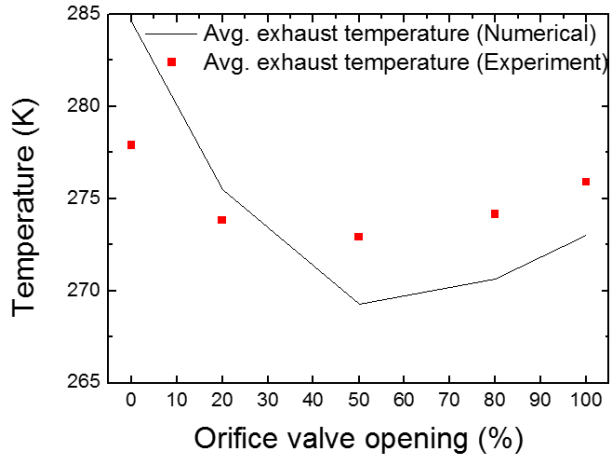

Fig. 6. Average exhaust temperature according to opening degree of orifice valve.

4.2. Experiment and numerical analysis at low temperature

In the low temperature experiment, the intake temperature is set at 220 K. As mentioned earlier, the gas is pre-cooled before entering the intake valve, and the intake temperature is controlled by a nichrome wire heater

TABLE 2
NUMERICAL AND EXPERIMENTAL CONDITIONS AT LOW TEMPERATURE. (IN EXPERIMENTS, THE EXPANSION TIME WAS 0.12 SECONDS)

Variable		Value
pulse tube	inner diameter	12.1 mm
	length	500 mm
	thickness	0.3 mm
	material	stainless steel
reservoir volume		500 cm³
diameter of intake valve		3 mm/ 0.22
diameter of exhaust valve		3 mm/ 0.26
initial temperature and pressure in reservoir & pulse tube		1 Bar/ 300 K
cycle period		0.36 s
intake time		0.06 s
expansion time		0.03, 0.06, 0.09, 0.12, 0.15, 0.18, 0.21, 0.24 s
high pressure/ low pressure		900 kPa/ 100 kPa
intake temperature		220 K
working fluid		gas nitrogen
diameter and opening degree of the orifice valve		1.42 mm 0, 20, 50, 80, 100 %

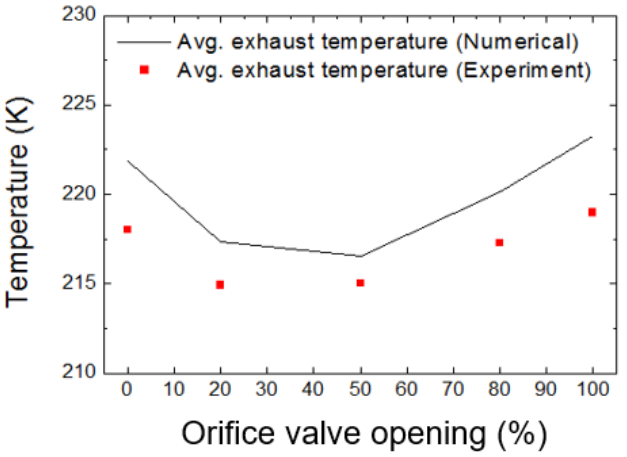

Fig. 7. Average exhaust temperature according to opening degree of orifice valve. (T_{in}=220 K)

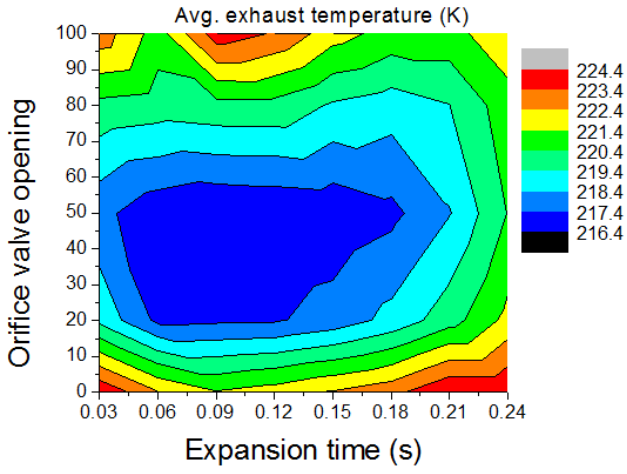

Fig. 8. Average exhaust temperature according to expansion time and orifice valve opening coefficient. (Tin=220 K) (Calculation)

installed in the intake line. The conditions for numerical analysis and experiment at low temperature are shown in TABLE 2. The experiment is carried out only for the case of 0.12-second expansion time. When the expansion time is 0.12 seconds, the average exhaust temperature according to the opening degree of the orifice valve is shown in Fig. 7. Fig. 8 shows the calculation results of the average exhaust temperature while varying the expansion time and the opening degree of the orifice valve.

From the above analysis, it is confirmed that the temperature of the exhaust gas does not decrease effectively in the case of low temperature experiment. The isentropic efficiency is about 3.6 % when the orifice valve opening is 50 %. This value is very low compared to the isentropic efficiency of 23.4 % at ambient temperature experiment. In some cases, it is shown that the exhaust temperature is higher than the intake temperature due to heat ingress by the solenoid valves and from the wall surface. In order to identify this cause of inefficient operation, we analyzed the exergy loss distribution and the results are presented in Fig. 9. Exergy is calculated by the following equation (8).

$$\Delta\boldsymbol{\varphi} = \boldsymbol{\varphi}_{exh} - \boldsymbol{\varphi}_{in} = (\boldsymbol{h}_{exh} - \boldsymbol{h}_{in}) + \boldsymbol{T}_0(\boldsymbol{s}_{exh} - \boldsymbol{s}_{in}) + \frac{\boldsymbol{V}_{exh}{}^2 - \boldsymbol{V}_{in}{}^2}{\boldsymbol{2}} \quad (8)$$

Exergy analysis shows that the exergy loss in the intake and exhaust valves account for 86.8 %, and the shuttle loss, which occurs due to the flow of gas from the warm end maintained at ambient temperature to the cold end, also occupies 10.9 %. Fig. 10 shows the result of numerical analysis of the temperature at the cold end during one cycle. During the exhaust process, it is found that the temperature of the cold end slightly decreases by the pressure drop, and then increases by the influence of the warm end. It is clear that the shuttle loss due to the flow from the warm end to the cold end has a significantly detrimental effect. Also, this effect is much greater at low temperature than at ambient temperature.

5. ADDITIONAL EXHAUST LINE

In order to reduce the influence of the warm end during the exhaust process, numerical analysis is examined by changing the exhaust time. Fig. 11 shows the results of the pressure in the pulse tube and the reservoir for one cycle with the exhaust time set to 0.18 seconds and 0.12 seconds, respectively, under the same conditions as in TABLE 2.

The average exhaust temperature is 216.5 K, 217.2 K for 0.18 second and 0.12 second respectively. As the exhaust time is shortened, the amount of the exhausted gas from the reservoir during the exhaust process is reduced maintaining high pressure in the reservoir. As a result, the pressure ratio of the pulse tube and the reservoir during the expansion process decreases.

For this reason, it is confirmed that the average exhaust gas temperature is higher than the case of 0.18 second when the exhaust time is 0.12 second. Therefore, we propose an innovative method to keep the pressure of the

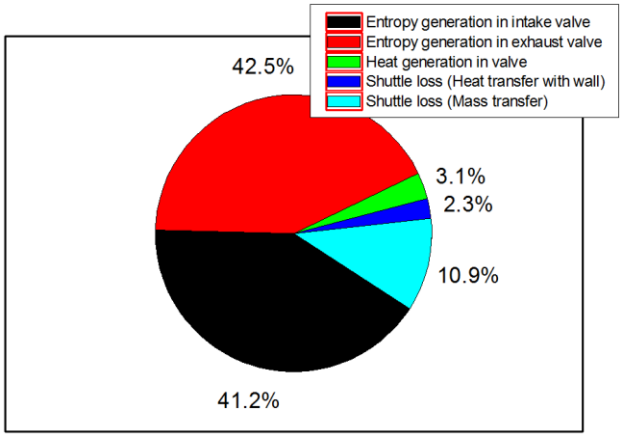

Fig. 9. Exergy loss rate of each factor (Calculation).

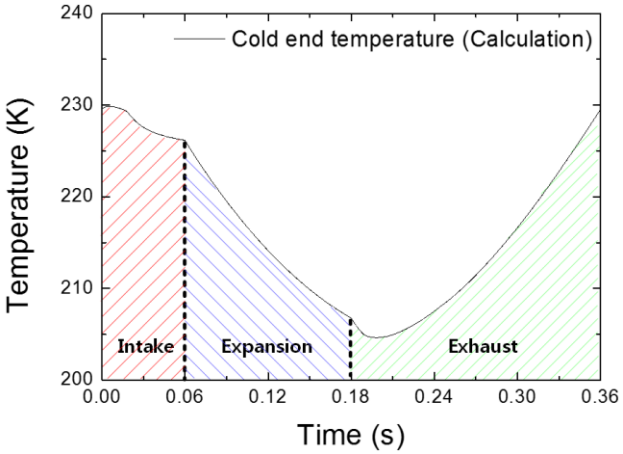

Fig. 10. Cold end temperature during one cycle in cyclic steady state. (orifice opening coefficient=50 %, T_{in}=220 K, intake/ expansion/ exhaust time=0.06/ 0.18/ 0.12 s)

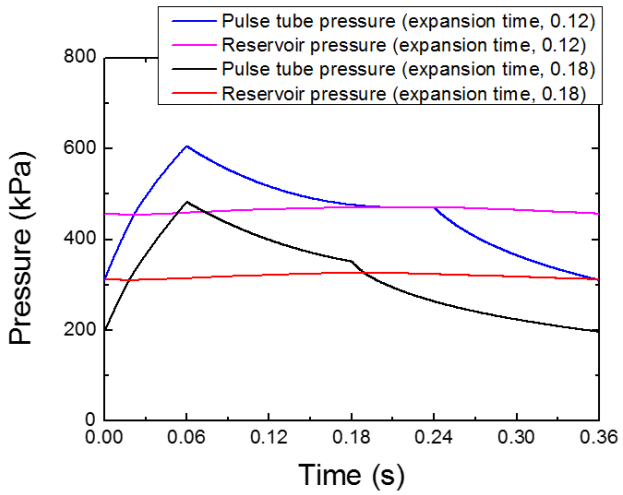

Fig. 11. Pressure during one cycle in cyclic steady state at each exhaust time (Calculation).

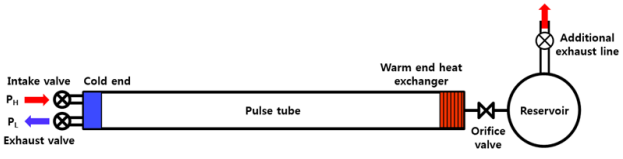

Fig. 12. Schematic of expander with additional exhaust line.

reservoir low by installing an additional exhaust line to the reservoir so that some gas exhaust from the reservoir to the outside during the expansion process. Experiment set-up including additional exhaust line is drawn as Fig. 13. Low-pressure gas leaving the reservoir enters the compressor through an expansion valve. The average exhaust temperature according to the orifice size of the additional exhaust line based on the conditions in TABLE 2 is examined in this new experiment set-up. The results are shown in Fig. 14. It shows that the average exhaust temperature significantly decreases by installing an additional exhaust line.

In our experimental set-up, there are several loss components such as irreversible pressure drop across the intake and exhaust valves, heat ingress from solenoid valves, and unwanted heat flow from the warm end to the cold end. If the diameter of the intake and exhaust valve increase from 3 mm to 9 mm and the expander operates between 500 kPa and 200 kPa instead of 900 kPa and 100 kPa, the pressure loss at both sides of the intake and exhaust valves decreases. This can reduce losses and increase isentropic efficiency of expander significantly. In the same condition as TABLE 2 except that the diameter of the intake and exhaust valve and the high and low pressure are changed, the isentropic efficiency changes according to the orifice size of the additional exhaust line as shown in Fig. 15. The isentropic efficiency is calculated by the following equation.

$$\varepsilon_{isentropic} = \frac{\dot{m}_{exh,act} \cdot (h_{in} - h_{exh})_{actual}}{\dot{m}_{total} \cdot (h_{in} - h_{exh})_{issentropic}} \tag{9}$$

From these results, it is confirmed that the isentropic efficiency is 38.4 (%) with additional exhaust line. This value is very large compared to the value in the preceding 3.6 % isentropic efficiency.

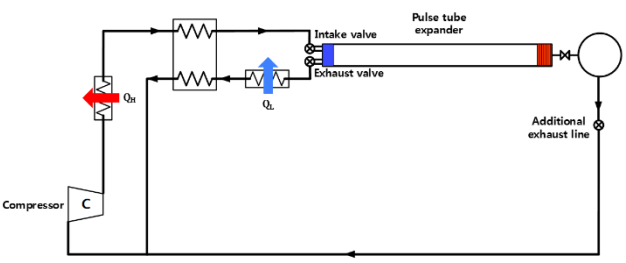

Fig. 13. Overall schematic with additional exhaust line.

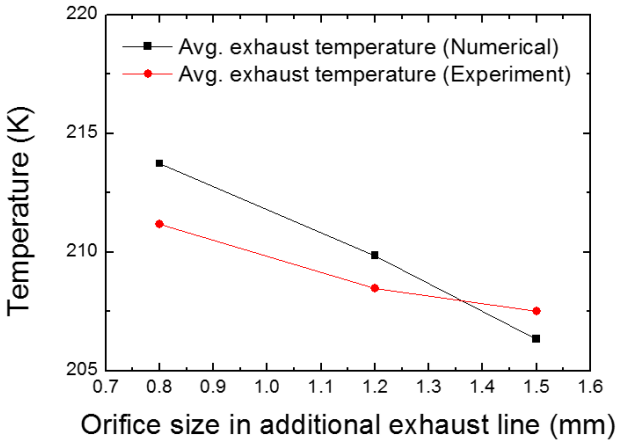

Fig. 14. Average exhaust temperature according to the orifice size of the additional exhaust line.

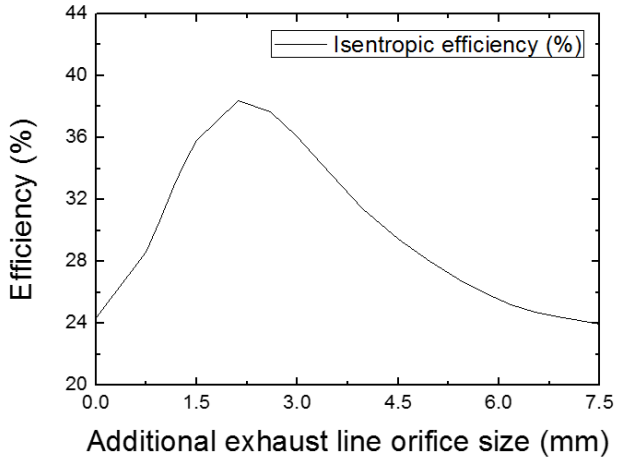

Fig. 15. Isentropic efficiency according to the orifice size of the additional exhaust line (intake & exhaust valve diameter: 9 mm, high & low pressure: 500 kPa & 200 kPa) (Calculation).

6. CONCLUSION

This paper describes the expander without moving parts and its numerical analysis. Experiments have been conducted to confirm its operation and identify the loss components. The numerical model is verified by the experimental results in both the ambient temperature and low temperature cases. It is shown that the efficiency of expander can be significantly increased when the additional bypass exhaust line is installed with no heat-generating valves under low pressure ratio of operation.

ACKNOWLEDGMENT

This work was supported by the National Research Foundation of Korea(NRF) grant funded by the Korea government(MSIT) (NRF-2017R1A2B3003152).

NOMECLATURE

ρ : Density of gas (kg/m^3)
$\dot{m}$: Mass flow rate of gas (kg/s)
A_g : Cross sectional area of pulse tube (m^2)
C_v : Volumetric specific heat (J/kg·K)
C_p : Isobaric specific heat (J/kg·K)
T_g : Temperature of gas (K)
h : Heat transfer coefficient (W/m^2·K)
A_s : Inner area of the pulse tube wall (m^2)
V : Volume of the pulse tube (m^3)
T_w : Temperature of the pulse tube wall (K)

P_{in} : High pressure (Pa)
P : Pressure in the pulse tube (Pa)
k : Conductivity of the gas (W/m·K)
k_w : Conductivity of the pulse tube wall (W/m·K)
A_w : Outer area of the pulse tube wall (m^2)
M_w : Mass of the pulse tube (kg)
C_w : Specific heat of the pulse tube wall (J/kg·K)
$\varepsilon_{isentropic}$: Isentropic efficiency (-)
$\dot{m}_{total}$: Total mass flow rate (kg/s)
h_{in} : Enthalpy of the intake gas (W)
h_{exh} : Enthalpy of the exhaust gas (W)
$\dot{m}_{exh,act}$: Mass flow rate only at exhaust valve (kg/s)
$\Delta\varphi$: Exergy difference (J)
φ_{exh} : Exergy of the exhaust gas (J)
φ_{in} : Exergy of the intake gas (J)
s_{exh} : Entropy of the exhaust gas (J/K)
s_{in} : Entropy of the intake gas (J/K)
V_{exh} : Entropy of the exhaust gas (m/s)
V_{in} : Entropy of the intake gas (m/s)

REFERENCES

[1] J J. Cha, J. Park, K. Kim, and S. Jeong, "Development of cryogenic free-piston reciprocating expander utilizing phase controller," *Progress in Superconductivity and Cryogenics*, vol. 18, pp. 42-47, 2016.

[2] C. L. Hannon, J. Gerstmann, B. J. Krass, M. J. Traum, J. G. Brisson, and J. L. Smith Jr., "Floating piston expander development for a small-scale Collins type 10 K cryocooler for space applications," *AIP Conference Proceedings*, vol. 710, pp. 1650-1660, 2004.

[3] J. Cha, "Development of cryogenic free-piston reciprocating expander utilizing phase controller," *KAIST, master's thesis*, 2016.

[4] J. Yuan and J. Pfotenhauer, "Thermodynamic analysis of active valve pulse tube refrigerators," *Cryogenics*, vol. 39, pp. 283-292, 1999.

[5] R. Radebaugh, "Development of the pulse tube refrigerator as an efficient and reliable cryocooler," *Institute off Refrigeration Proceedings*, vol. 96, 2000.

[6] S. Zhu, Y. Kakimi, K. Fujioka, and Y. Matsubara, "Active-buffer pulse-tube refrigerator," *Proceedings of the Sixteenth International Cryogenic Engineering Conference/International Cryogenic Materials Conferenc*e, pp. 291-294, 1997.

[7] Z. Gan, W. Dong, L. Qiu, X. Zhang, H. Sun, Y. He, and R. Radebaugh, "A single-stage GM-type pulse tube cryocooler operating at 10.6 K," *Cryogenics*, vol. 49, pp. 198-201, 2009.

[8] K. Wang, S. Dubey, F. Choo, and F. Duan, "Modeling of pulse tube refrigerators with inertance tube and mass-spring feedback mechanism," *Applied energy*, vol. 171, pp. 172-183, 2016.

[9] Y. Kim, "Study on the layered active magnetic regenerative refrigerator with multi-magnetic refrigerant," *KAIST, Ph.D thesis*, 2012.

[10] A. Cengel and M.Cimbala, Fluid mechanics, *Fundamentals and Application*, McGrawHill, 2006.

[11] P. Incopera, P. Dewitt, L. Bergman and S. Lavine, *Principles of heat and mass transfer: 7th ed*., Wiley, 2013.